



HAL
open science

Microstructure influence on the oxidation behaviour at 750°C of astroloy

C. Mons, C. Lineau, C. Haut, G. Rautureau, E. Beauprez, G. Moulin

► **To cite this version:**

C. Mons, C. Lineau, C. Haut, G. Rautureau, E. Beauprez, et al.. Microstructure influence on the oxidation behaviour at 750°C of astroloy. *Journal de Physique IV Proceedings*, 1993, 03 (C9), pp.C9-85-C9-97. 10.1051/jp4:1993906 . jpa-00252336

HAL Id: jpa-00252336

<https://hal.science/jpa-00252336>

Submitted on 4 Feb 2008

HAL is a multi-disciplinary open access archive for the deposit and dissemination of scientific research documents, whether they are published or not. The documents may come from teaching and research institutions in France or abroad, or from public or private research centers.

L'archive ouverte pluridisciplinaire **HAL**, est destinée au dépôt et à la diffusion de documents scientifiques de niveau recherche, publiés ou non, émanant des établissements d'enseignement et de recherche français ou étrangers, des laboratoires publics ou privés.

Microstructure influence on the oxidation behaviour at 750 °C of astroloy

C. Mons⁽¹⁾, C. Lineau⁽¹⁾, C. Haut⁽¹⁾, G. Rautureau⁽²⁾, E. Beauprez⁽²⁾ and G. Moulin⁽¹⁾

⁽¹⁾ Laboratoire de Métallurgie Structurale, ISMA, URA 1107, Bâtiment 413, Université Paris XI, 91405 Orsay, France

⁽²⁾ ETCA, CREA/PS-LA, 16 bis Avenue Prieur de la côte d'Or, 94114 Arcueil, France

Abstract. — γ - γ' nickel base alloy, as Astroloy is sensitive to environment for fatigue crack propagation at 750 °C. Two main oxides are obtained, especially enriched with Ni, Al (+Cr) in the outer zone and with Al, Cr in the inner one. The oxide scale growth is mainly controlled by oxygen bulk diffusion, except in the case of rolled sample where a linear diffusion of oxygen can also intervene for the growth of inner oxide layer. The inner oxide scale grows 10^3 times faster than the outer one. On account of the different diffusivities of metal and oxygen together with the dissolution of oxygen and formation of suboxides, (containing Ni, Cr in γ phase and Al, Ti in γ' islands) at the oxide scale-alloy matrix interface, an accumulation of mechanical constraints occurs in the alloy during oxidation. With a model based on "a solutal elastic effect when the concentration of solute varies" [1] a depth corresponding to a maximum stress was estimated between 3.4×10^{-8} cm to 1154×10^{-8} cm in front of the oxide scale-alloy matrix interface. Local enrichment in oxygen on induced defects (vacancies, holes) or precipitates then disturb the ^{18}O diffusion profile *versus* alloy's depth.

1. Introduction.

In the case of many nickel base alloys for aerospace applications there occurs a strong interaction between environment and mechanical properties, not only for usual tensile tests (with slow strain rate of 0.5 mm/min [2]) but also during fatigue crack growth measurements [3, 4]. The environmental influence is mainly linked with the specific effect of oxygen diffusing along the grain boundaries and allowing: physico-chemical evolution due to embrittling segregated elements, microstructural transformations (in relation with new phase formation or induced precipitation) mechanical perturbations (especially on account of the weakening of atomic bonds associated with oxygen content increase or oxygen chemisorption). The protective behaviour of surface oxide scales against oxygen penetration into the alloy is then essential. The oxygen barrier compartment of the scale is really dependant upon the composition, internal stresses, microstructure of each oxide layer on the surface [5, 6].

The aim of the present study is then embedded with the growth mechanism of oxide scale (s) and oxygen diffusion in Astroloy (γ - γ' Ni base alloy) with new industrial applications required up to 750 °C, i.e. in a temperature range where the oxygen influence might be enlarged [7]. All the previously mentioned chemical, kinetical, microstructural and mechanical aspects of oxidation will be studied both according to the atmosphere (air, pure oxygen, oxygen containing water vapor) and to the alloy's treatment (cold rolling, then annealing). The

last parameter might give accurate informations both on the oxidation behaviour of strained parts of the alloy (such as crack tips) and on the influence of defects in the diffusion process of oxygen.

2. Material.

The alloy was elaborated from prealloyed powder (REP), then consolidated by extrusion at 1100 °C (γ' solvus = 1135 °C) leading to 60% of γ' phase. The composition of the alloy and different phases (γ and γ') are reported in table I. Different solutionning (near the solvus) and aging cycles (700 °C-800 °C) are then performed as reported in a previous paper [7]. An average γ grain size of nearly 60 μm is then obtained, with γ' size of nearly 0.2-0.3 μm . Some samples are cold rolled (= 50%), then annealed in argon for 70 h at 800 °C with Ti-Zr getters.

Table I. — *Composition of the base alloy and of the different γ and γ' phases (weight %).*

éléments	C	Ni	Co	Cr	Al	Ti	Mo	B	Zr
alloy	0,028	55,56	16,9	14,9	4,1	3,4	5,1	0,02	0,05
γ		44,7	23,1	22,9	1,7	0,6	6,8		
γ'		71,2	8,6	3,3	7,5	7,1	2,3		

3. Experimental procedure.

Many techniques are used for this study: optical or/and scanning electron microscopy; transmission electron microscopy with dispersive energy analyses (STEM + EDAX), X-ray photoelectron spectroscopy (XPS) with Ar^+ sputtering at rates of 50 nm/h (also used as "angular analyses"); secondary ion mass spectroscopy (primary ions gas (Ar^+), energy = 10 keV, $I_p = 50$ nA, secondary ions $V = 4500$ V, analysed area = 62 μm , balayage raster = 250 μm , contrast aperture = 150 μm). The oxidation kinetic is studied both using sample weight evolutions (Cahn Thermobalance apparatus of sensitivity = + or - 10 μg) and oxygen $^{18}\text{O}_2$ diffusion in a specific plant (enabling successive oxidations in $^{16}\text{O}_2/^{18}\text{O}_2$ atmosphere, with $p\text{O}_2 = 0.4$ atm.).

4. Microstructural and analytical study of as received samples, before oxidation.

The main influence of the rolling, then annealing treatment is the formation in some places of γ grains elongated along the rolling deformation axis. As for the unrolled sample, the average size of γ grains is 60-80 μm . In both cases γ' surstructure appears as small islands of nearly 200-300 nm average width surrounded with γ phase (Fig. 1a). The γ phase is enriched with small precipitates of γ' and $(\text{Mo}, \text{Cr})_{23}\text{C}_6$ in the case of unrolled samples [8]. After rolling, then tempering, the γ grain boundaries look like jagged (Fig. 1b) and enriched with small carbides containing Cr and Mo, while big $(\text{Cr}, \text{Mo})_{23}\text{C}_6$ particles are formed in

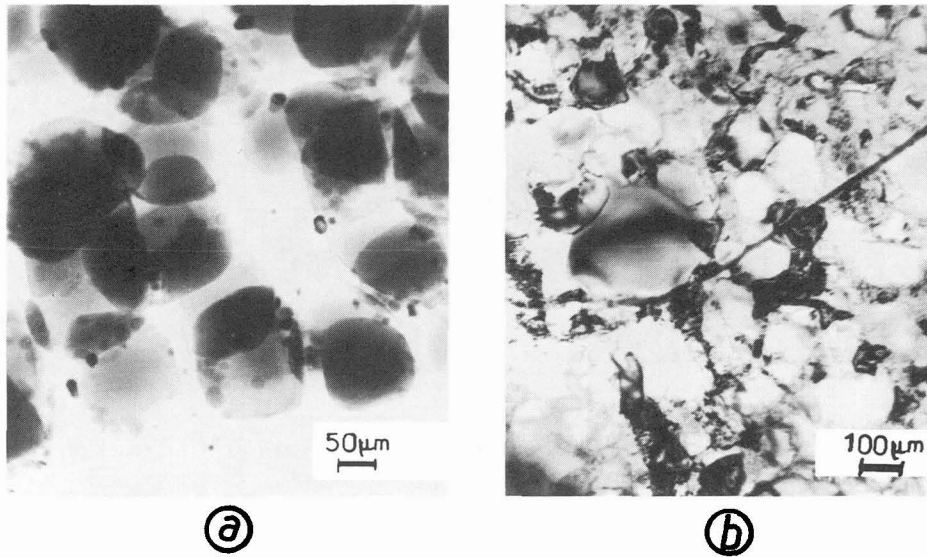


Fig. 1. — Microstructures of rolled and unrolled Astroloy: a) Initial Astroloy. Islands of γ' and small precipitates between γ' ; b) Rolled Astroloy. Big precipitates of $(\text{Mo}, \text{Cr})_{23}\text{C}_6$ in the alloy's bulk.

others microstructural places (Fig. 1b). The linear defect content increases, especially in the γ phase between γ' islands.

5. Microstructural and analytical study after oxidation. Outer oxidation.

- After oxidation in oxygen, a quite homogeneous oxide scale grows on the surface, with preferential cracks straight on the grain boundaries of the underlying alloy (Fig. 2a). In air or oxygen with water vapor, for as received samples, as in oxygen for rolled samples, the oxide scale is inhomogeneous, especially in relation with many spalled oxide areas (as white zones in Fig. 2b).
- XPS angular spectroscopy analyses related to the very thin outer oxide layer obtained in air (Fig. 3b) complete the first results after oxidation in pure oxygen (Fig. 3a) [8]: the nickel content increases while the Al percentage is slightly lowered than in oxygen $p\text{O}_2 = 1$ atm).

6. Evolution of the element percentage through the oxide layer.

- More deeply into the oxidized area, accurate informations are also obtained using the same XPS spectroscopic analysis, and especially the binding energy shifts of the elements and thin relative content evolution through the oxide layer (after successive Ar^+ sputterings). In the case of oxidation in oxygen and air, for rolled and unrolled samples, the primary oxide layer (near the surface) is especially enriched with oxidized Al, Ni (and Cr) while the inner one mainly contains Al and Cr (+ Co) in oxidized state (Fig. 4a, b, c). In air, or for rolled sample, the distinction between the primary and secondary oxidized areas is more evident.
- SIMS depth profiles agree with these element evolutions through the oxidized layer as observed for instance in figure 5 showing a high nickel signal in the outer oxidized zone,

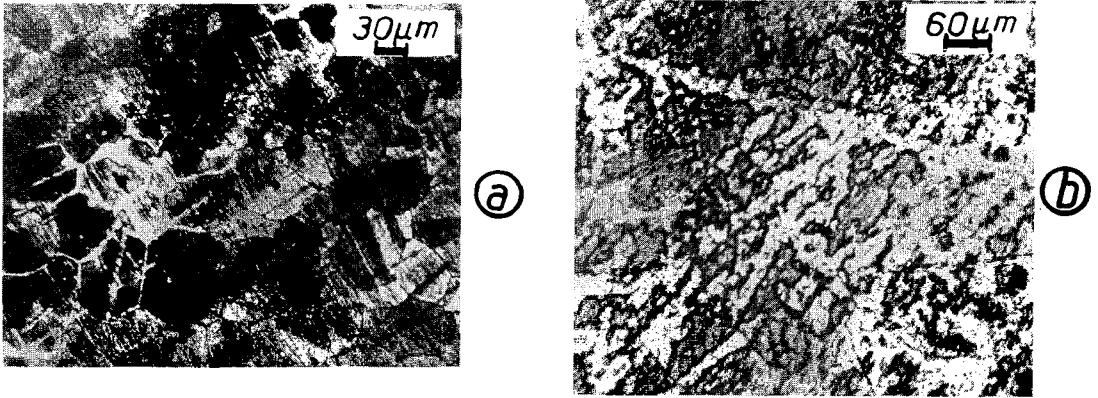


Fig. 2. — Morphology of the oxide scale after oxidation of 1 h in O_2 at $750^\circ C$: a) crack on the surface of unrolled Astroloy; b) spalled areas on the surface of rolled samples.

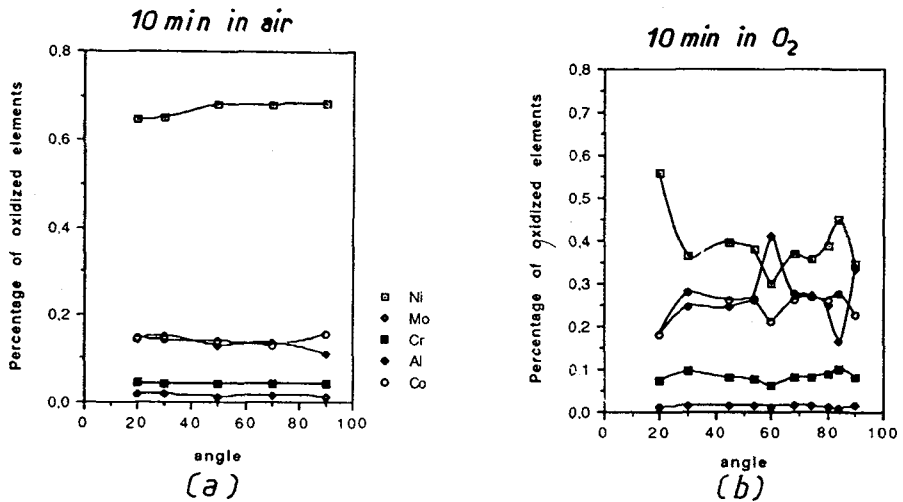


Fig. 3. — XPS analysis giving the percentage of oxidized elements *versus* sample-detector angle for: a) Astroloy oxidized 10 min in O_2 ; b) Astroloy oxidized 10 min in air.

then an increase of Cr and Al intensities in the inner oxidized area into the alloy. The width of the zone containing Al extends with the oxidation time, or in the case of oxidation of rolled sample.

In the case of oxidation in pure oxygen with water vapor (25 ppm), there is a large increase of the respective percentage of oxidized Ni, Cr and Ti at the prejudice of oxidized Al (at least in the outer oxidized zone (Fig. 4d)).

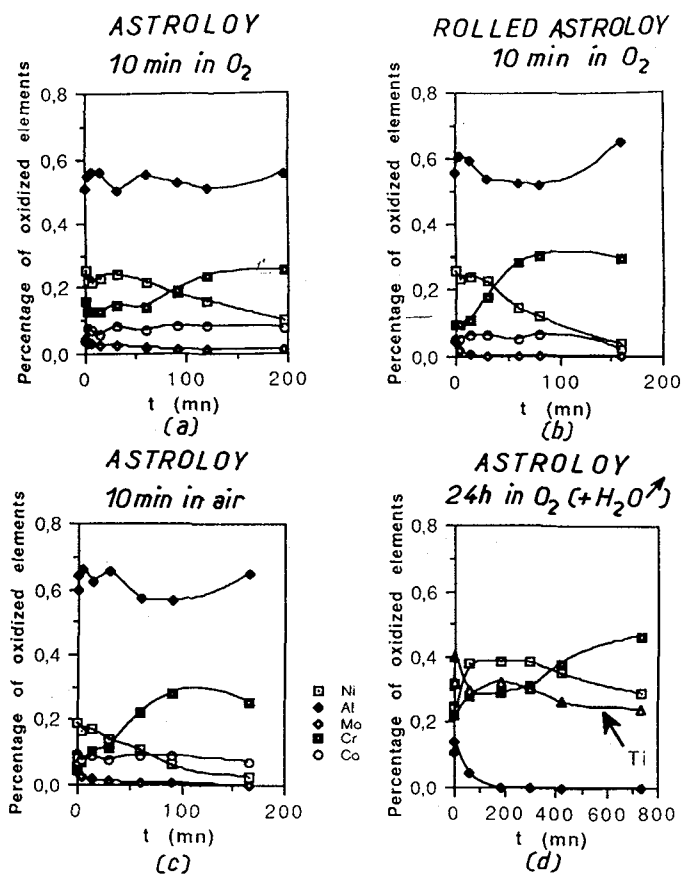


Fig. 4. — XPS analyses of the percentage of oxidized elements *versus* Ar⁺ sputtering time (i.e. oxide or alloy's depth).

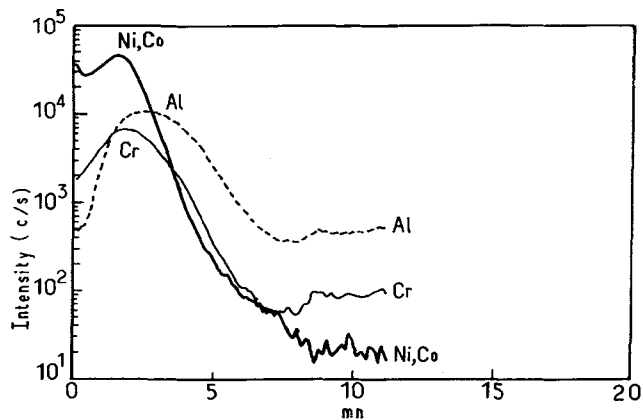


Fig. 5. — SIMS profile of elements in Astroloy oxidized for 3 h in ¹⁸O₂ then 1 h in ¹⁶O₂.

7. Relation between microstructure and local enrichments in oxidized elements.

• SIMS images at nearly 300-500 Å depth into the outer wholly oxidized zone – as proved by ^{18}O images – show that enrichment in Al-O and Cr-O associations take place not only at the grain boundaries, but also in some particular places of the grain bulk (Fig. 6).

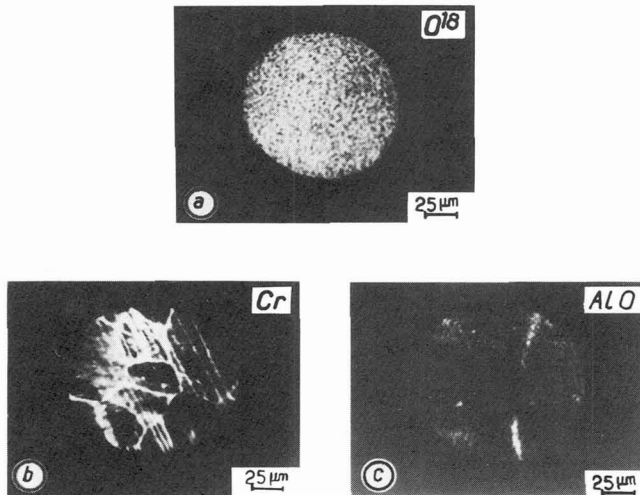


Fig. 6. — SIMS images of elements at 500 Å from the surface of Astroloy, precoated with ^{18}O , then annealed for 3 days in vacuum: a) homogeneous distribution of ^{18}O ; b) enrichment of chromium at the grain boundaries; c) enrichment of aluminium both at the grain boundaries and in alloy's bulk.

• More accurate analyses of the interaction between precipitates and microstructure were performed on thin oxidized foils in air, i.e. at depths between 1.5-2.5 μm from the initial surface after sample thinning: NiCr_2O_4 or hexagonal Cr_2O_3 particles were observed in γ phase whereas Al_2O_3 oxides were analyzed in γ' islands [8, 9]. STEM analyses of figures 7a, b confirm the increase of the chromium percentage straight on the γ phase and the enhancement of the Cr, Ti, Al content at the grain boundaries in such an oxidized zone, for instance after oxidation for 40 h in air at 750°C. In case of the rolled sample oxidized in air, there happens a slight evolution of the Co, Cr and Mo content at the grain boundaries. Big precipitates observed in the alloy's bulk are no more enriched with Mo, but always contain a high Cr content with respect to the γ phase (Figs. 8b, c).

8. Kinetic study. Oxide scale(s) growth.

Successive reoxidation steps are observed during annealing in oxygen whereas for rolled samples, in air, a first oxidation step is followed by weight loss, then no more weight change (Fig. 9). In oxygen containing 25 ppm water vapor, the main observation concerns a quick and sharp weight loss before the sequence of slight and discontinuous oxidation (Fig. 9). Parabolic rate constants, k_p , can always be calculated in the first oxidation time, sometimes in a second domain (Tab. II). Oxidation kinetic enhances in the case of rolled samples and

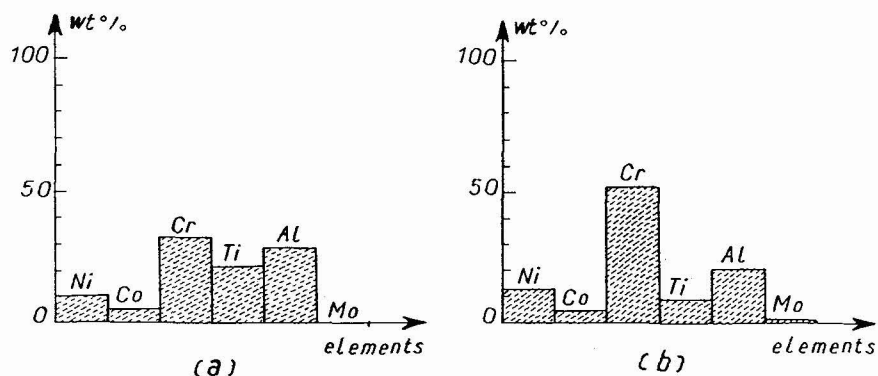


Fig. 7. — STEM analyses of different structures in Astroloy oxidized for 40 h in air at 750 °C: a) zone with precipitates; b) grain-boundary.

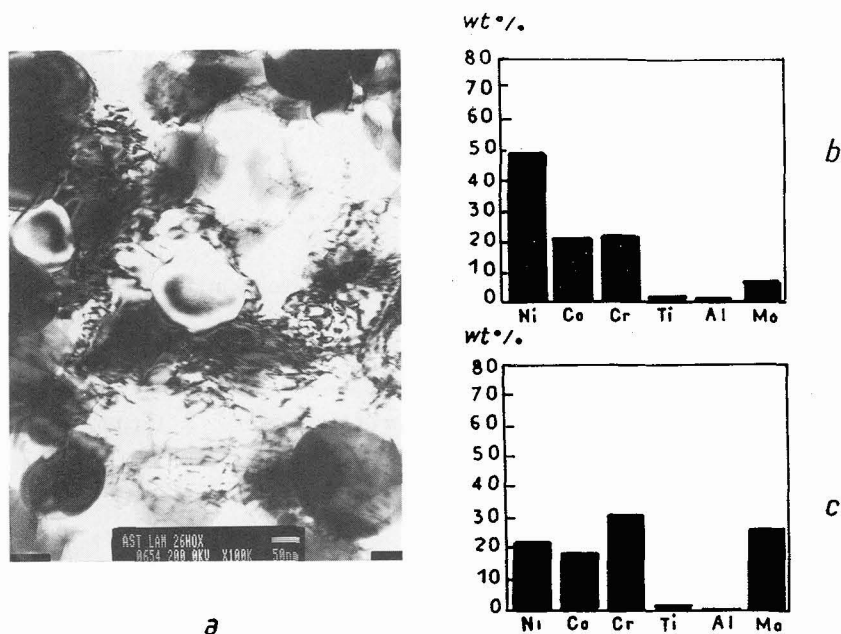


Fig. 8. — Microstructural and STEM analyses after oxidation in air at 750 °C: a) oxidized bulk of Astroloy after oxidation for 26 h in air at 750 °C; b) STEM analysis in the oxide; c) STEM analysis in a zone with big precipitates.

is faster in air than in oxygen. For the most obvious oxidation phenomenon (first oxidation step of rolled sample), an activation energy of oxidation of 259 kJ/mole can be drawn out.

9. Oxygen penetration through the outer oxide scale.

From the SIMS analyses of the evolution of ^{16}O and ^{18}O intensities versus Ar^+ sputtering time, and with respect to oxide depths obtained from thermogravimetric study and height

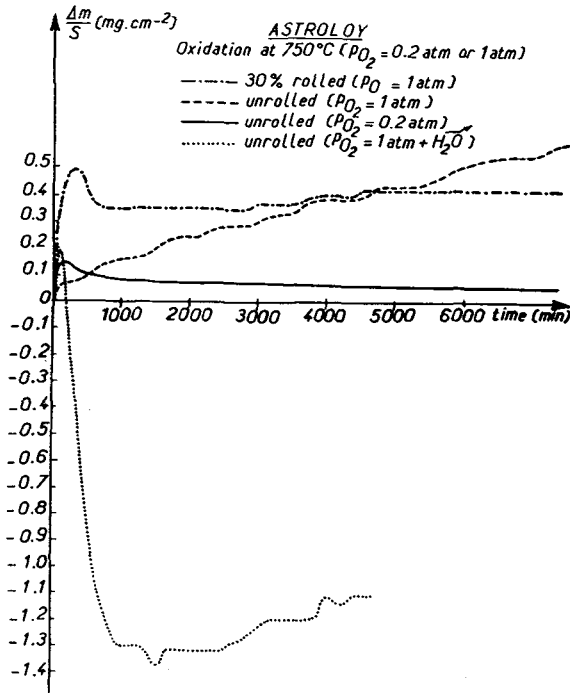


Fig. 9. — Weight change *versus* oxidation time at 750 °C of Astroloy in different atmospheres or after mechanical pretreatment.

Table II. — Apparent parabolic constants of oxidation of Astroloy at 750 °C (in $g^2/cm^4.s$).

alloy	atmosphere	oxygen ($pO_2=1$ atm)	air
unrolled	1rst domain	5.10^{-13}	2.10^{-12}
unrolled	2nd domain	$(6-10).10^{-13}$	
rolled	1rst domain	5.10^{-12}	5.10^{-12}
rolled	2nd domain	5.10^{-13}	$(1-7).10^{-13}$

measurements of sputtered craters, the ratio $^{18}O / (^{16}O + ^{18}O)$ is plotted *versus* oxide depth after oxidation in $^{16}O_2$, then $^{18}O_2$ at 750 °C (Fig. 10a). A comparison is made with the ^{18}O profile *versus* oxide thickness, in case of diffusion from a thin layer into a semi-infinite area (Fig. 10b).

– In case of bulk diffusion of ^{18}O through the outer oxide scale, a diffusion law according to Argerf $((C - C_s) / (C_o - C_s)) = f(x)$ is valid, which corresponds to an isotopic exchange model with a constant value of diffusing element on the outer surface. C is the oxygen content at every layer depth x , C_s the oxygen content on the surface and C_o the oxygen content at

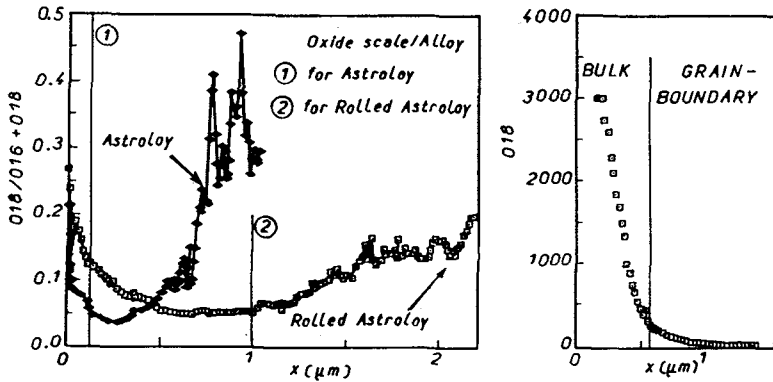


Fig. 10. — SIMS analyses of the: a) evolution of the percentage of ^{18}O versus the depth into Astroloy and rolled Astroloy after oxidation for 3 h in $^{16}\text{O}_2$ then 1 h in $^{18}\text{O}_2$; b) diffusion profile of ^{18}O from a thin surface deposit of ^{18}O after annealing of 3 days in vacuum at 750°C in Astroloy.

the infinite. The initial conditions (for $t = 0$) are $X > 0, C(X, 0) = C_0$ or the natural ^{18}O isotopic content in the oxide. The limit conditions are: $t > 0, X = 0, C(0, t) = C_s$ with C_s = oxygen content on the surface.

When plotting the oxide scale depth versus the probability $100 - 1/2(C/C_s)$, the slope of the curve m can give the diffusion parameter D_v , according to $D_v = m^2/2t$ (with t = diffusing time). (cf. Fig. 11a, for instance)

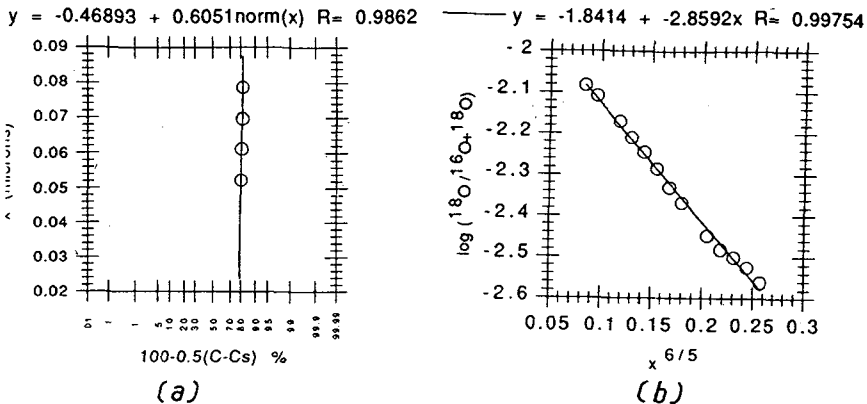


Fig. 11. — a) The oxide scale depth versus the probability $100 - 1/2(C/C_s)$; the slope of the curve m can give the diffusion parameter D_v , according to $D_v = m^2/2t$. b) Curve which the slope $d \log (^{18}\text{O}/^{16}\text{O} + ^{18}\text{O}) / dx^{6/5}$ and give the diffusion parameter $D_j\delta$, according to the Wipple-Le-Claire equation.

– When ^{18}O intergranular diffusion prevails the apparent intergranular diffusion parameter $D_j\delta$ is deduced from the Wipple-Le Claire [10] law according to:

$$D_j\delta = 0.661 \left(\frac{-\text{dlog } x_c}{\text{d}x^{6/5}} \right)^{-5/3} \left(\frac{4 D_v}{t} \right)^{-1/2}$$

with x = oxide layer depth, x_c = ^{18}O percentage, D_v = bulk diffusion, t = diffusion time. An example of such a curve is given in figure 11b. The different results are reported in table III.

Table III. — Evolution of the diffusion parameters (D_v , $D_j\delta$) of ^{18}O as a function of alloy treatment.

Treatment	unrolled sample	rolled sample	
	3h $^{16}\text{O}_2$ +1h $^{18}\text{O}_2$	25' $^{16}\text{O}_2$ +12' $^{18}\text{O}_2$	3h $^{16}\text{O}_2$ +1h $^{18}\text{O}_2$
oxidized area			
outer zone	(D_v) 8.10^{-16} $\text{cm}^2.\text{s}^{-1}$	(D_v) $2,3.10^{-13}$ $(\text{cm}^2.\text{s}^{-1})$	(D_v) $3,4.10^{-14}$ $(\text{cm}^2.\text{s}^{-1})$
inner zone	(D_v) $5,1.10^{-13}$ $\text{cm}^2.\text{s}^{-1}$	$D_j\delta=(1,5-3).10^{-26}$ $\text{cm}^3.\text{s}^{-1}$	$D_j\delta=(0,4-5).10^{-25}$ $\text{cm}^3.\text{s}^{-1}$

10. Discussion.

A previous work gave informations on the growth mechanism of the very outer oxide layer [8]. This indicates the formation of two inner oxide layers: the outer (or primary one) containing mainly Al and Ni (Cr); the inner (or secondary one) enriched with Al and Cr especially. Calculations of each parabolic rate constant was made using Hale's model [11] elaborated in case of duplex oxidation, i.e. when a primary oxide scale forms together with a quite impervious healing (or secondary) oxide layer especially growing at hemispherical grain boundaries. The total weight gain per unit surface area (ΔW_I) and the second one (ΔW_{II}) is given by the relation:

$$\Delta W (t < t_c) = \Delta W_I + \Delta W_{II} = (k_I t)^{1/2} - \frac{\rho_I^2}{3r^2} (k_I t)^{3/2} + \frac{\pi}{2r} \rho_I (k_I t)^{1/2} (k_{II} t)^{1/2}$$

with ρ_I : constant of proportionality related to oxide density.

$k_{I(II)}$: primary (secondary) parabolic rate constant.

t_c : critical time, when penetration reaches the depth r (or final depth of the primary scale = 500 Å)

k_I is measured from microstructural and analytical evolution as 3×10^{-16} g/cm² in oxygen. Then the parabolic rate constant for the growth of the secondary oxide scale is found as $k_{II} = 1.5 \times 10^{-13}$ g/cm².

The shift between k_I and k_{II} of nearly 10^3 times is of the same order than for the bulk diffusion parameters of ^{18}O between the outer and the inner oxide scales (cf. Tab. II). This

constatation supports the activation energy of 259 kJ/mole for the outer oxide growth (or rolled sample) which is usually related to a growth mechanism controlled by oxygen diffusion.

For the rolled samples, in the deeper oxidized zone of the alloy, the linear diffusion of oxygen may be explained by the increasing influences of new interfaces (big precipitates, strained interfaces of γ' islands) and linear defects in the γ phase.

Artefacts observed in the oxygen diffusion profiles *versus* oxidized alloy's depth (local and heterogeneous increases of oxygen) are explained by an accumulation of mechanical stresses in the alloy during metal and oxygen diffusion together with formation of suboxides (NiCr_2O_4 , Cr_2O_3 , (Ti, Al, Cr) oxides, Al_2O_3) and dissolution of oxygen at the oxide scale-alloy interface.

The theory which is used is based on a solutal elastic effect when the concentration of solute varies at this interface where the transfert of metal and oxygen also induced diffusive vacancies [1, 12]. In the model, the steady concentration balance in front of the interface of the thin layer is based on Fickian equations taking into account the linear contribution to the rate of formation of suboxide and of oxygen dissolution kC_{ox} (with (C_{ox} = oxygen content)) and the velocity V of the relative oxide surface motion.

On account of the sink term kC_{ox} , an apparent coefficient D_{ox}^* smaller than D_{ox} is introduced as [1]:

$$D_{\text{ox}}^* = 2D_{\text{ox}} \left(1 + \left(1 + \frac{4kD_{\text{ox}}}{V^2} \right)^{1/2} \right)^{-1}$$

Associated with the matter balance in such a dominant anionic diffusion, a stress field is generated with a maximum value at a portion z_{max} inside the alloy's bulk according to [1]:

$$z_{\text{max}} = \frac{D_{\text{M}} D_{\text{ox}}^*}{D_{\text{M}} - D_{\text{ox}}} + 1/V \log e \frac{-\alpha_{\text{ox}} \Delta C_{\text{ox}}(\text{O}) D_{\text{M}}}{\alpha_{\text{M}} \Delta C_{\text{M}}(\text{O}) D_{\text{ox}}^*}$$

With D_{M} , D_{ox} = diffusion parameters of metal, oxygen

α_{M} , α_{ox} = dilational coefficients of alloy ($0.3 \times 10^{-6} \text{ }^\circ\text{C}^{-1}$) and oxide ($9.6 \times 10^{-6} \text{ }^\circ\text{C}^{-1}$)

$\Delta C_{\text{ox}}(\text{O})$, $\Delta C_{\text{M}}(\text{O})$ = variation in oxygen or metal concentrations at the oxide scale-alloy interface (O).

The results are reported in table IV for unrolled and rolled oxidized alloys. This maximum stress calculated near the oxide scale-alloy interface, especially for oxidation in pure oxygen of unrolled sample, could then induce the formation not only of oxide precipitates and linear defects, but also of holes from the vacancies generated during the outer scale growth in Ni Al base alloys [12]. Direct observation of such porosity was effectively made at this oxide-alloy interface on short angle transverse section of oxidized sample (Fig. 12). As a confirmation without surface oxidation no heterogeneous and local enrichment in ^{18}O is observed in the alloy (compare Fig. 10a,b). For the oxide scale spalling both mechanical properties evolution of the alloy (in the case of rolled sample) and chemical evolution of the oxide scale (oxidation in air or oxygen with water vapor of unrolled sample) could be evoked. It remains a much debated question up to now. In both case, the common result is the formation of a more dissociate inner oxide layer than in the case of oxidation in oxygen (cf. Fig. 3). The modification of the volume per oxide mole between the inner oxide containing especially Al and Cr and the outer one enriched with Ni and Al might then induce a more important Pilling Bedworth effect.

Table IV. — Portion of the maximum z_M of the constraint inside the alloy matrix-oxygen as a function of the heat treatment (in air or oxygen) at 750 °C of rolled and unrolled alloys.

alloy parameters	unrolled sample		rolled sample
V (cm.s ⁻¹)	$3,6.10^{-7}$	$1,96.10^{-7}$	$6,4.10^{-7}$
D_{Ox} (cm ² .s ⁻¹)	10^{-12}	10^{-12}	10^{-12}
$D_{Ni,Cr}$ (cm ² .s ⁻¹)	3.10^{-14}	3.10^{-14}	6.10^{-14}
k ()	150	150	110
D^*_{ox} (cm ² .s ⁻¹)	$2,9.10^{-14}$	$2,7.10^{-14}$	$5,9.10^{-14}$
z_M (cm)	456.10^{-8}	$3,4.10^{-8}$	1154.10^{-8}

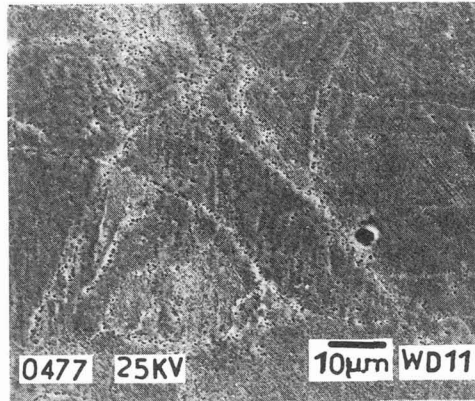


Fig. 12. — Scanning electron microscopy on sectionned sample of Astroloy at the end of the inner oxidized zone, showing precipitates and especially holes or bubbles both at the grain boundaries and in the alloy's bulk.

11. Conclusion.

Oxidation of Astroloy mainly takes place *via* inwards oxidation. Two main oxidized zones are obtained: the outer one enriched especially with Ni, Al (+Cr) and the inner one containing Cr and Al. For oxidation of unrolled samples, oxygen bulk diffusion is essential and oxygen penetration strongly slows down through the outer oxide scale with respect to the inner oxide layer (10^3 times lesser). The same decreasing factor of 10^3 is observed for the oxidation rate constant relative to each oxide scale at 750 °C in pure oxygen ($pO_2 = 1$ atm). For rolled samples, oxidation is increased at least during a first annealing step where activation energy indicates a scale growth control by oxygen. Then the large contribution of linear diffusion of oxygen was attributed to the influence of all defects (linear defects, precipitates) observed after rolling.

In front of the oxidized zone, in the alloy's matrix chromium precipitates are formed in γ phase and Al (+Ti) enriched oxides in γ' phase and at the grain boundaries (+Cr). A maximum stress field is calculated near the inner oxide scale alloy interface, which favours oxide precipitation and hole formation, then local enrichment in oxygen (artefacts in ^{18}O percentage evolution *versus* alloy's depth). Chemical evolution of the outer oxide scale (in air) or mechanical properties modification of the base alloy (rolled samples) cannot explain alone oxide scale spallings.

Acknowledgements.

The authors would like to thank particularly Drs M. Marty, R. Mevrel, M. Walder, M. Pichoir (ONERA, Chatillon sous Bagneux, France) for many discussions concerning this work. Drs C. Monty and C. Dolin are also acknowledged for microstructural and analytical (SIMS) studies.

References

- [1] SANFELD A., HENNENBERG M., BERTRAND G., CANNOT J.C., *Corros. Sci.* **28** (1988) 1163.
- [2] SHAHINIAN P., *Trans. ASME* **6** (1965) 344.
- [3] PANDEY M.C., TAPLIN D.M.R., ASHBY M.F., DYSON B.F., *Acta Metall.* **34** (1986) 2225.
- [4] SADANANDA K., SHAHINIAN P., *J. Mater. Sci.* **13** (1978) 2347.
- [5] HUPPSLEY C.A., STRANGWOOD M., DE VAN J.M., *Acta Metall. Mater.* **38** (1990) 2393.
- [6] HOU P.Y., STINGER J., *Acta Metall. Mater.* **36** (1991) 841.
- [7] MONS C., MOULIN G., *High Temperature Materials for Power Engineering*, Vol. II (Kluwer Academic Publishers, 1990) p. 1205.
- [8] MOULIN G., MONS C., SEVERAC C., HAUT C., RAUTUREAU G., BEAUPREZ E., Analytical study of surface and bulk oxidation of Astroloy, submitted to *Surface and Interface Analysis* (1992).
- [9] WHITTLE D.P., SHIDA Y., WOOD G.C., STOTT F.M., BASTOW B.D., *Philos. Mag. A* **46** (1982) 931.
- [10] LE CLAIRE A.D., *Br. J. Appl. Phys.* **14** (1963) 351.
- [11] SMITH A.F., TUCKER M.O., HALES R., *Oxid. Met.* **17** (1982) 329.
- [12] FRASER H.L., SMALLMAN R.E., LORETTO M.H., *Philos. Mag.* **28** (6) (1973) 651.
- [13] ROUSSELET J.M., Influence d'une prédéformation et des impuretés S et C sur la résistance à l'oxydation d'un alliage $\text{Ni}_{76}\text{Cr}_{16}\text{Fe}_8$ (Inconel 600), Doctor Thesis (Orsay, France, 30 Juin 1988).